J. Fluid Mech. (1991), *vol.* 226, *pp.* 205–217
Printed in Great Britain

Trapped internal waves over undular topography

By C. KRANENBURG[1], J. D. PIETRZAK[2]† AND G. ABRAHAM[2]

[1] Department of Civil Engineering, Delft University of Technology, PO Box 5048, 2600 GA Delft, the Netherlands

[2] Delft Hydraulics, PO Box 177, 2600 MH Delft, the Netherlands

(Received 22 November 1989 and in revised form 11 September 1990)

We describe observations of slowly decelerating stratified flow over undular bottom topography in an estuary. The flow, which initially was supercritical with respect to the first internal wave mode, approached a resonance after it had become subcritical. A series of acoustic images showed large-amplitude first-mode trapped waves during this phase of the tide. We derive a criterion for quasi-steady response, and present an extension of Yih's class II linear finite-amplitude solutions that accounts for the waves observed.

1. Introduction

The flow of a stratified fluid over an obstacle may generate various phenomena, most notably lee wave formation and upstream influence, which have been the subject of experimental and theoretical studies for several decades. Of the many reviews available, those by Baines (1977, 1984), Huppert (1980) and Turner (1973) are particularly relevant.

Attention in this paper is focused on slowly decelerating stratified flow over undular topography as observed in a tidal channel of restricted depth, see figure 1. The flow and density distribution are two-dimensional and horizontally quasi-periodic. The undulations of the bed (a series of ridges) have a wavelength that is typically larger than the water depth, while their height is only a small fraction of the water depth. The flow is internally supercritical initially and passes into the internally subcritical regime thereafter. Restricting the discussion to first vertical-mode internal waves, criticality is defined here in the hydraulic sense, that is, the flow is critical when the upstream first-mode long-wave speed vanishes with respect to a fixed coordinate system. If a horizontal axis is taken in the direction of the flow, the speed of this long wave will be positive in supercritical flow and negative in subcritical flow.

1.1. *Conceptual model of resonant trapped waves*

In comparison to the flow over a single obstacle, the stratified flow over an undulating bed seems to have received little attention in the literature. However, it appears to be possible to describe, at least in a qualitative sense, the flow over a series of identical obstacles starting from the literature on a single obstacle. The study of Baines (1984) on two-layer flow is of particular interest in this connection, because of its relative completeness and emphasis on upstream influence. Other references are Grimshaw & Smyth (1986) and Melville & Helfrich (1987).

In the case where the undisturbed interface is at mid-depth (this case

† Present address: Department of Oceanography, University of British Columbia, Vancouver, BC, Canada V6T 1W5.

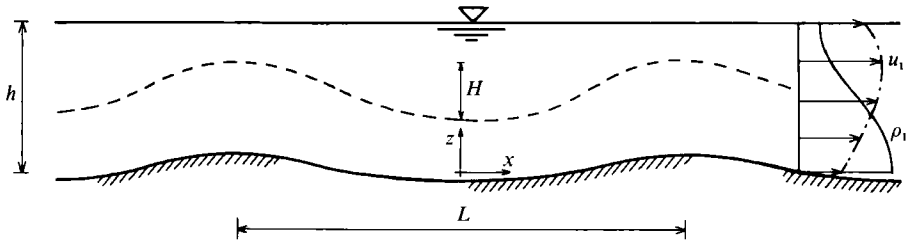

FIGURE 1. Schematic diagram of flow configuration investigated: ——, horizontally averaged density profile $\rho_1(z)$; —·—·—, horizontally averaged velocity profile $u_1(z)$; – – – –, typical streamline. The (flood) current is in the landward direction.

approximately represents the observed density structure when modelled as a two-layer system), there will be no upstream influence so long as the flow is supercritical, see figure 8(*e*) in Baines (1984). The flow then is largely determined by the local topography and there is no interaction with the flow over the other obstacles. As the flow (slowly) decelerates, it becomes subcritical at a certain instant and, as a consequence, wave disturbances (of type 5E or 5C in Baines 1984) start to travel in the upstream direction from each obstacle. At this stage the flow would tend to become transcritical, that is, subcritical upstream and supercritical downstream of each obstacle. As a result the interface downstream would drop. The flow downstream of a particular obstacle constitutes the upstream boundary condition for the next obstacle, so that Baines' results for smaller ratios of lower-layer depth to water depth would now apply. His figure 8 (*a–d*) shows that for finite obstacle heights the wave disturbances succeed in propagating in the upstream direction. These waves reach the obstacle upstream after some time, which causes the flow to become subcritical everywhere. The transcritical flow regime is only transient. With a finite series of obstacles this argument applies to all but the last (most downstream) obstacle, where the flow remains transcritical for a much longer time.

As the flow continues to slow down, resonance conditions arise at the instant when the upstream speed of a first-mode internal wave, the wavelength of which equals that of the topography, becomes zero. A resonance can develop in subcritical flow only, since waves of finite wavelength generally travel more slowly than the long waves mentioned, which have a wavelength that goes to infinity. Simple linearized steady-state theory predicts large-amplitude trapped internal waves when the flow is near-resonant, but finite-amplitude effects then can no longer be ignored.

Maxworthy (1979), and Lansing & Maxworthy (1984) showed that in decelerating tidal flow lee waves downstream of a single obstacle may start to propagate over the topography. In the case of a series of obstacles as considered here, the trapped waves over downstream obstacles may play a similar role. However, this mechanism cannot develop so long as the flow is not yet at resonance, because free waves with the wavelength of the topography then would still travel in the downstream direction.

The argument leading to the possibility of resonance requires the flow to decelerate gradually. More specifically, the travelling time, τ_w, of the upstream wave disturbance from one obstacle to the other should be much less than the time interval, τ_r, between critical flow and resonant flow. Approximating the speed c of a first-mode internal wave for large (but finite) wavelengths L by $c \approx -U + c_0[1-\alpha(h/L)^2]$, where U is the mean water velocity, h the mean water depth, α a coefficient of order one, and c_0 the wave speed for $L \to \infty$ in water at rest, the flow is critical when $U = U_c = c_0$ and resonant when $c = 0$ or $U = U_r = c_0[1-\alpha(h/L)^2]$. At resonance the speed of a long wave in the upstream direction is $-U_r + c_0 = \alpha c_0 (h/L)^2$.

The travelling time τ_w therefore is $L/[c_0(h/L)^2]$, to an order of magnitude. The time interval τ_r is of the order $(U_c - U_r)/|dU/dt|$, where t is time. On the assumption that $|dU/dt|$ is of order $c_0\omega$, where ω is the tidal frequency, τ_r becomes of order $(h/L)^2/\omega$ [note that for small $(h/L)^2$ the time τ_r is small compared to the tidal period ($\sim 1/\omega$)]. Introducing a characteristic buoyancy frequency N so that $c_0 \sim Nh$, the condition for quasi-steady subcritical flow becomes

$$\left(\frac{L}{h}\right)^5 \frac{\omega}{N} \ll 1 \quad (h/L < 1). \tag{1.1}$$

An approach which is seemingly more straightforward is to substitute the quasi-steady linear solution in the time-dependent linearized basic equations, and to estimate the error thus made. However, a weaker condition $[(L/h)\omega/N \ll 1]$ then results. The difference from (1.1) is caused by the implicit disregard in a linearized model of upstream influence, which is an intrinsically nonlinear effect.

Bell (1975) examined the oscillatory stratified flow over an obstacle on the bed of an otherwise unrestricted water body, and proposed $\omega/N \ll 1$ as a condition for quasi-steady behaviour. Bell's calculations indicate that this condition can be relaxed substantially, which, however, does not necessarily apply to the corresponding condition (1.1).

1.2. *Outline of paper*

The observations of the first-mode trapped internal waves referred to were made in a shallow stratified estuary during decreasing flood (Pietrzak, Abraham & Kranenburg 1989; Pietrzak, Kranenburg & Abraham 1990). In §2 we describe the measuring site, and present mean density and velocity profiles as well as some acoustic images showing large-amplitude trapped waves. Next, in §3 we give a quasi-steady finite-amplitude analysis for a Boussinesq fluid based on Yih's (1980) class II linear solutions of the exact stream function equation. This class of solutions includes the solution given by Long (1953). The solution obtained holds for subcritical flow; it is not intended to correspond completely with the observations, but serves mainly for comparison. Finally, in §4 we make some concluding remarks.

2. Field observations

The measurements were made in the Rotterdam Waterway, a man-made channel that discharges fresh water from the River Rhine into the North Sea. Following the usual classification with respect to the density structure (e.g. McDowell & O'Connor 1977), this estuary varies from stratified during neap tides and high river discharges to partially mixed during spring tides and low discharges. The measuring site selected was located in a slightly curved reach of the estuary at km 1016. The local width between the groynes is 350–380 m, the navigation channel is 250 m wide, and, depending on position, the water depth near the axis was 16.3–18.0 m at the time of the measurements. Echo-sounding and side-scan sonar recordings showed the presence of a pronounced series of thirteen permanent ridges at the bed with their crests at approximately right angles to the axis of the navigation channel. The wavelengths vary from 28 to 74 m and the heights of the ridges from 1.15 to 1.80 m. These ridges extend from at least 50 m south to 25 m north of the axis. They have formed on an elevated section of the bed, the difference in the levels being about 1.5 m.

The data to be presented here were obtained on the decreasing flood during a normal tide and a relatively high river discharge on 21 October 1987. Vertical profiles

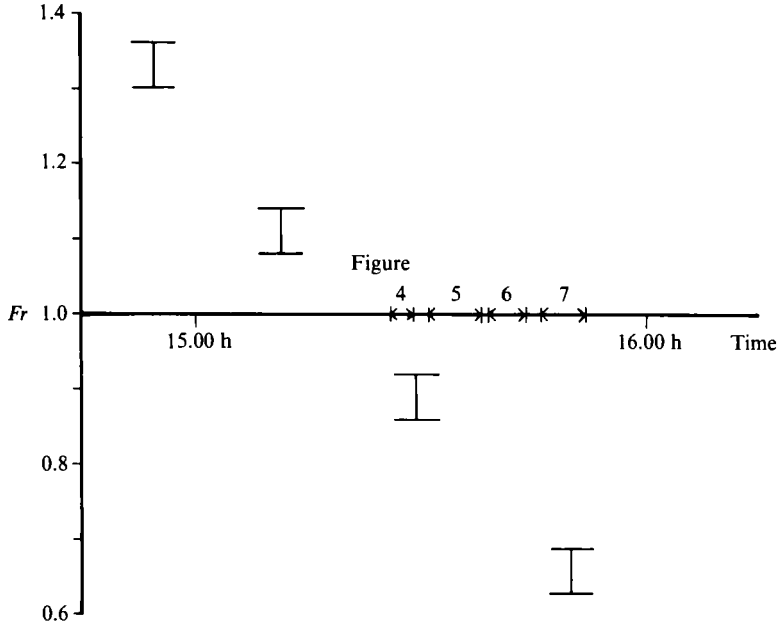

FIGURE 2. Internal Froude numbers calculated from the measured data versus time. The flow is internally supercritical for $Fr > 1$, and subcritical for $Fr < 1$. The periods when the acoustic images shown in figures 4–7 were taken are indicated.

of density and horizontal velocity were measured using conductivity and temperature meters and an impeller-type current meter from a survey vessel anchored at the axis of the waterway at km 1016. One-minute averages were obtained to eliminate high-frequency fluctuating components in the signals. The densities were calculated from the conductivities and temperatures. At the same time a second vessel recorded acoustic images of the density structure as well as the bed using a 210 KHz transducer while sailing up and down along the axis, or parallel to it, between km 1015.5 and km 1016.5.

2.1. *Results*

Estimates of an internal Froude number Fr defined as

$$Fr = \frac{U}{c_0} \tag{2.1}$$

are shown as a function of time in figure 2. The initially supercritical flow became subcritical to first-mode waves at about 15.20 h (MET), where upon the possibility of resonance arose. We shall concentrate on the period 15.23–15.57 h, because the wave pattern as shown on the acoustic images then was clearly related to the topography. Considerable internal-wave activity also existed at other instants, but the acoustic images then showed the large spatial and temporal variability inherent to many geophysical flows. Sometimes internal waves due to cargo vessels interfered with the observations.

In the time interval selected two sets of velocity and density profiles were taken, see figure 3. The low near-surface velocities can be attributed to the gravitational circulation: the longitudinal density gradient along the estuary drives a net (tidally averaged) circulation in vertical planes that is directed landward near the bed and seaward near the free surface (e.g. Chatwin 1976; McDowell & O'Connor, 1977).

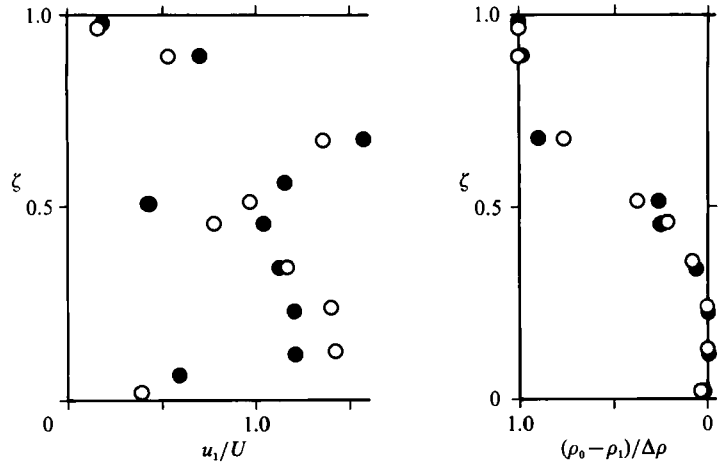

FIGURE 3. Observed velocity (u_1) and density (ρ_1) profiles: ○, 15.23–15.36 h, $U = 0.44$ m/s, $\Delta\rho = 10.2$ k/m^3; ●, 15.42–15.57 h, $U = 0.36$ m/s, $\Delta\rho = 11.4$ kg/m^3.

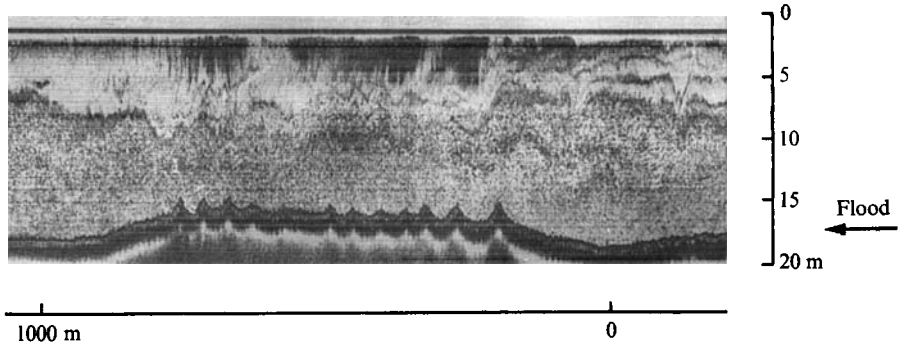

FIGURE 4. Acoustic image taken about 25 m north of the axis of the waterway while sailing up the estuary from 15.26–15.29 h. The flood current is from right to left. Water depth and horizontal distance in m.

Consequently, relatively low near-surface velocities result during flood. The reduced velocities at the level of the halocline were observed only when trapped internal waves were present. Such a dip in the velocity profile may be attributed to the deformation of the flow due to the waves: if the current meter is just beneath a crest, or just over a trough of a first-mode trapped internal wave, the measured velocity will be less than in a situation where the wave is not there. Thus the measured velocity profiles are contaminated with wave components. If it is assumed that the flow is quasi-steady, see §1.1, the measured profiles should be representative of the flow including possible upstream effects of the ridges. The density profiles show nearly homogeneous layers near the free surface and the bed, and a diffused halocline. Blocking of the flow is not to be expected because of the nearly constant density across the (small) height of the ridges. Estimated values of the gradient Richardson number at the halocline are of the order of one, indicating stable stratification.

The first acoustic image in this period was taken about 25 m north of the axis of the waterway from 15.26–15.29 h, see figure 4. At this position the ridges are less pronounced, but nevertheless trapped first-mode waves had started to develop. This is shown more clearly in the second image (15.31–15.38 h), figure 5. This and the next

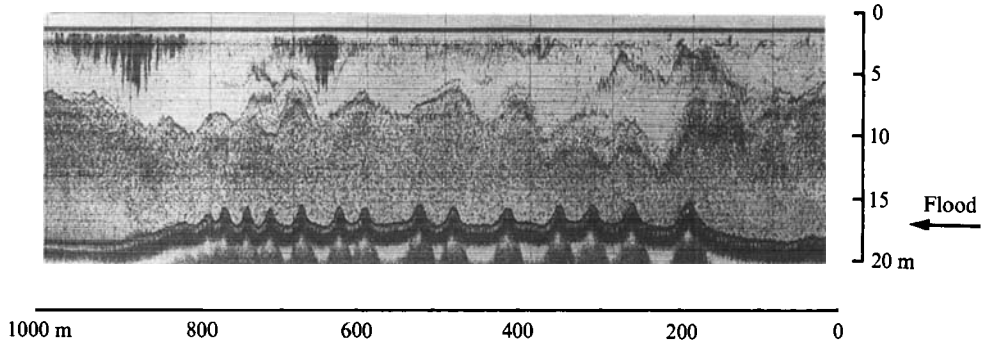

FIGURE 5. Acoustic image taken along the axis of the waterway from 15.31–15.38 h.

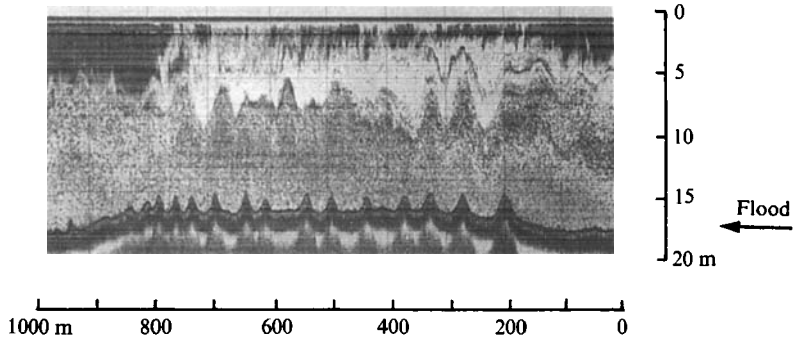

FIGURE 6. Acoustic image taken along the axis of the waterway from 15.39–15.44 h.

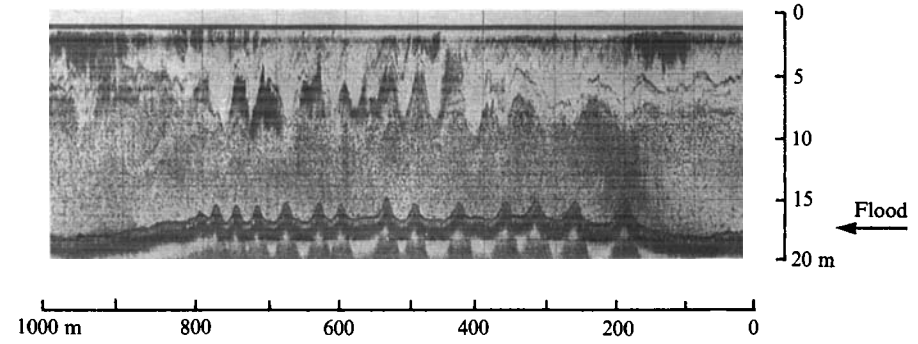

FIGURE 7. Acoustic image taken along the axis of the waterway from 15.46–15.52 h.

two images were taken along the axis. It was verified that the grey-tones on the images do represent density differences by towing a conductivity meter through the wave train. Variations in density so obtained can be converted into vertical displacements of streamlines by using a mean-density profile taken simultaneously.

In figure 5, large-amplitude trapped first-mode waves have arisen over the ridges, but in some cases the wave seems to respond to two adjacent ripples as if they were a single topographic feature. The order-of-magnitude argument of § 1.1 indicates that the resonant wavelength $L \sim h/(\omega\tau_r)^{\frac{1}{2}}$, whence it may be concluded that initially the flow reacts mainly to long-wave components of the topography. Increasingly smaller resonant wavelengths are to be expected as τ_r increases.

The course of events proposed seems to be in accord with the two acoustic images taken from 15.39–15.44 h (figure 6) and 15.46–15.52 h (figure 7), which seem to show more trapped waves over single ridges. Also, the response to the relatively isolated

first ridge (counted from the seaward side, that is, the first from the right in figure 6), which is quite strong on the second and third images, has diminished by the time of the fourth image, figure 7.

Figures 6 and 7 reveal first-mode waves of large height, up to 6.6 m, which is 40% of the water depth (over the fifth ridge in figure 7) or 5 times the height of the ridge. The maximal steepness (wave height/wavelength) is about 0.11, and maximal angles of inclination of the halocline are about 30°. The crests of waves and ridges coincide in most cases, which is typical of a flow that is nearing resonance from the supercritical side. The dimensionless parameter $(L/h)^5\omega/N$ in (1.1) is about 0.02 for the smallest wavelengths and about 3 for the largest ones, so that at least the shorter waves should be in quasi-steady equilibrium.

After resonance, part of the trapped-wave system appeared to disintegrate showing waves of smaller amplitude, which were not uniquely coupled to the topography. These waves therefore may have been developing lee waves. On the seaward side of the series of ridges there was some evidence of first-mode waves, the wave-length of which was roughly that of the topography. This may have been a manifestation of the mechanism proposed by Maxworthy (1979), see §1.1. Internal waves showing inverted profiles (with the troughs of the waves over the crests of the ridges), which are characteristic of a subresonance response, developed over some of the ridges. The interpretation of these observations is further complicated by a flow reversal near the free surface driven by the gravitational circulation, shortly after the acoustic image of figure 7 was taken. However, critical-layer phenomena were not evident. For example, the inclined wave structures below the critical layer observed by Koop & McGee (1986) were absent. The data obtained in this phase of the tide are not sufficient to analyse the internal-wave response in greater detail.

3. Finite-amplitude trapped-wave model

A theoretical description of near-resonant trapped internal waves over a periodically corrugated bed is presented in this section making use of an extension given by Yih (1980) of Long's (1953) linear finite-amplitude solution of the exact stream-function equation for two-dimensional flow. This solution does not allow one to prescribe arbitrary velocity and density profiles, and therefore is not intended to correspond with the data in all respects. It is given merely for comparison and to explain the resonant waves of the height observed. Referring to §1.1, we consider the subcritical flow regime only.

Some numerical calculations using the Taylor–Goldstein equation for small-amplitude disturbances, together with appropriate boundary conditions at a sinusoidal bed and a horizontal free surface, as well as observed velocity and density profiles, were also carried out (Pietrzak *et al.* 1990). The calculated wavelengths of the bed at which resonance occurs (for a given Froude number) were found to compare well with those resulting from the model discussed in the section to follow. This is not surprising, since for the wavelengths of interest the dispersion relations are not widely different. As expected, the wave heights predicted by the small-amplitude and finite-amplitude models agree so long as the wave height is small. However, the small-amplitude model was found to overestimate the wave heights in near-resonance conditions. In a particular case (the case with $A = 0$ in figure 9) the error at the onset of gravitational instability is about 45%. Therefore, the linear finite-amplitude model is preferable for the present purpose. An alternative would be to solve a non-linear initial-value problem numerically.

We ignore real-fluid effects and three-dimensionality caused by the finite lengths of the ridges. The density variations are assumed to be small. The method applied is indirect in the sense that the shape of the topography is not prescribed at the outset, but is calculated afterwards from the solution considered. However, the wavelength and height of the topography are prescribed.

3.1. *Formulation*

Adopting the Boussinesq approximation, the stream function ψ corresponding to Yih's class II solutions satisfies an equation which for the present application can be written as

$$\nabla^2\psi + \frac{b^2}{h^2}\psi = \frac{\pi^2 U}{h^2 F^2}(z + A'h), \tag{3.1}$$

where U is the mean (horizontally and depth-averaged) water velocity and A' is a constant. The Froude number F, which in general differs from the Froude number Fr defined by (2.1), is given by

$$F^2 = \pi^2 \frac{U^2}{(\Delta\rho/\rho_0)\, gh}. \tag{3.2}$$

Here $\Delta\rho$ is the top to bottom density difference and ρ_0 is the density at the bed. The constant b is given by

$$b^2 = \left(2\pi \frac{h}{L}\right)^2 + \frac{\pi^2}{(1+a)^2}. \tag{3.3}$$

The solution given by Yih is extended here by introducing the constant a ($0 < a \ll 1$). It is shown below that the extended solution allows for the undular bottom topography.

The stream function is of the form $\psi = \psi_1 + \psi_2$, where ψ_1 represents, for the case under consideration, the horizontally averaged flow and ψ_2 the trapped wave. These stream functions are given by

$$\psi_1 = \pi^2 \frac{Uh}{b^2 F^2}[\zeta - A \sin b\zeta + A'(1 - \cos b\zeta)] \tag{3.4}$$

and, for a mode-one wave as observed,

$$\psi_2 = \pi^2 \frac{Uh}{b^2 F^2} B \cos\xi \sin \pi \frac{\zeta + a}{1 + a}, \tag{3.5}$$

where $\xi = 2\pi x/L$ and $\zeta = z/h$ are dimensionless horizontal and vertical coordinates ($\zeta = 0$ at the undisturbed bed and $\zeta = 1$ at the free surface, which is approximated by a rigid lid), and A and B are constants. On substitution (3.4) and (3.5) are found to satisfy (3.1), provided the constant b is given by (3.3).

The boundary conditions at the bed and the free surface are $\psi = 0$ and, since U is the depth-averaged velocity and h the water depth, $\psi = Uh$. Together with (3.2) the latter expression gives

$$F^2 = \frac{\pi^2}{b^2}[1 - A \sin b + A'(1 - \cos b)]. \tag{3.6}$$

The density distribution is given by

$$\rho = \rho_0 - \frac{\Delta\rho}{Uh}\psi. \tag{3.7}$$

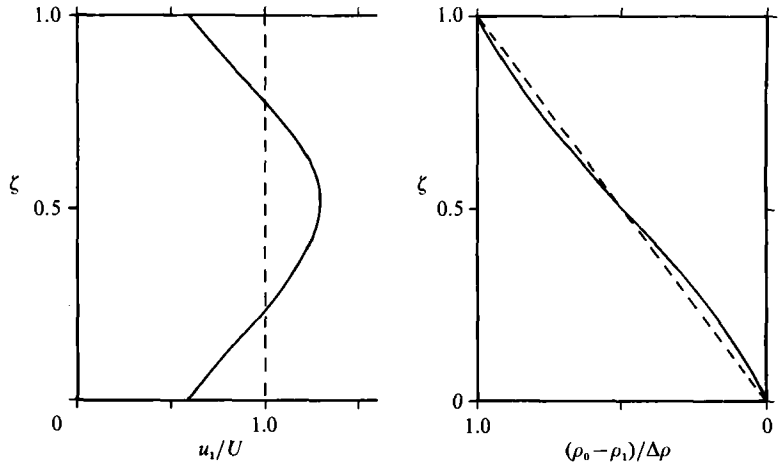

FIGURE 8. Theoretical horizontally averaged velocity and density profiles. Results are shown for $L = 30$ m, $h = 16.6$ m and $Fr = 0.676$ ($a = 0.02$), and closely approximate the profiles for other wavelengths and Froude numbers. ——, $A = 0.07$; – – – –, $A = 0$.

In general a compromise has to be sought to match both the observed velocity profile and the observed density profile, since (3.7) must be satisfied for the stream-function equation to become linear.

Results will be presented only for the case where the horizontally averaged velocity profile is symmetrical with respect to mid-depth $[\partial\psi_1(\zeta)/\partial\zeta = \partial\psi_1(1-\zeta)/\partial\zeta]$, see figure 3 for comparison. The constant A' then becomes $A' = -A\tan(\frac{1}{2}b)$ so that the Froude numbers F and Fr satisfy

$$Fr = \frac{F}{(1+2A')^{\frac{1}{2}}} = \frac{\pi}{b}. \tag{3.8}$$

The above expressions imply that the elevation $\zeta = \eta_b$ of the bed (where $\psi = 0$) is given by an expression of the form

$$f(\eta_b,\ \cos\xi; B, a, h/L, A) = 0. \tag{3.9}$$

The wave height $\Delta_b = (\eta_b)_{\xi=\pi} - (\eta_b)_{\xi=0}$ of the bed, the ratio h/L and the profile coefficient A being known from the observations, a relation between B and a results. The Froude number Fr also depends on a, so that a unique relationship between the parameters B and Fr exists.

A wave height, H, is defined as follows. The difference, η, in the displacement of a streamline at $\xi = 0$ and $\xi = \pi$ ($x = \frac{1}{2}L$) follows from

$$\psi(0,\zeta) = \psi(\pi, \zeta+\eta). \tag{3.10}$$

The maximum of η as a function of ζ (for $\zeta = \zeta_m$, say) is defined as the dimensionless wave height $H/h = \eta_m$,

$$\psi(0,\zeta_m) = \psi(\pi, \zeta_m+\eta_m). \tag{3.11}$$

η_m and ζ_m depend on B and a, hence on the Froude number Fr.

3.2. *Comparison with observations*

Theoretical velocity and density profiles for $A = 0$ and $A = 0.07$ are shown in figure 8. The velocity profile for $A = 0.07$ mimics the observed low near-surface and near-bottom velocities in figure 3, but as discussed in §2.1 does not reproduce the dip near

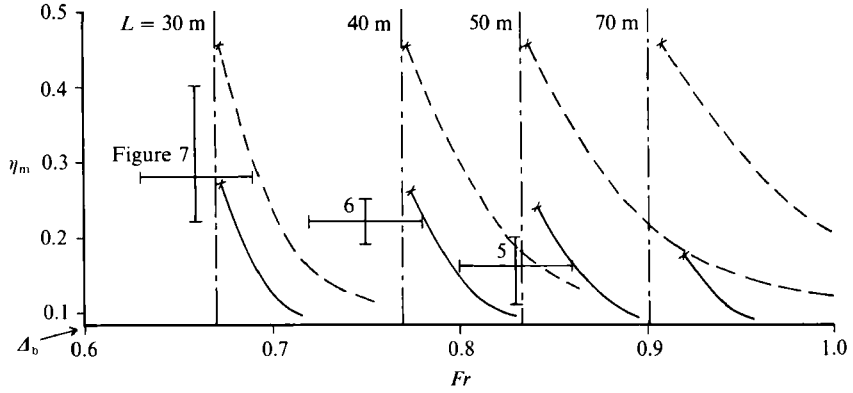

FIGURE 9. Observed and calculated wave heights versus internal Froude number. The observations indicated by error bars are based on the Froude numbers shown in figure 2 and the acoustic images of figures 5, 6 and 7. The vertical error bars represent the scatter in the measured wave heights. The calculations are for $h = 16.6$ m and $\Delta_b = 0.0831$. —— $A = 0.07$; – – –, $A = 0$; – · – ·, resonance; ×, onset of gravitational instability.

mid-depth. The observed nearly homogeneous layers near the bed and the free surface cannot be represented by this model. Attempting to prescribe zero density gradients at $\zeta = 0$ and $\zeta = 1$ would lead to an unrealistic velocity profile and gravitational instability over a non-flat bed. In addition to unsteadiness, three-dimensional and real-fluid effects, this fact renders the model of an approximate nature only. Baines (1984) remarks that the overall mode-one response for linear stratification is similar to that for a two-layer fluid with equal layer depths. Therefore, the discrepancy in the density profiles may be not too serious. To compensate for the different density profile, the model value of $\Delta\rho$ was chosen so as to make the theoretical Froude numbers Fr equal to the measured values.

Figure 9 shows, for various topographical wavelengths L, the calculated wave heights when Fr (slowly) decreases to approach resonance conditions. The results are seen to be sensitive to the profile coefficient A, which is not surprising because low near-bed velocities should result in a reduced response.† All theoretical curves terminate, before resonance conditions are met, when gravitational instability renders the theory invalid. Regions of stagnant fluid or rotors would then be expected to develop, but these were not observed, possibly because of the different density distribution. The observations shown in figure 9 correspond with the images of figures 5–7. The Froude numbers were obtained by interpolation. The theory predicts resonance for $L = 50 \pm 6$ m (conditions of figure 5), $L = 38 \pm 4$ m (figure 6) and $L = 29 \pm 2$ m (figure 7). However, the images show large wave heights for other wavelengths as well, which is likely to be a consequence of the variability of the flow. The model is reasonably successful in producing large waves not unlike those observed, and the calculations for $A = 0.07$ fit the data better than those for $A = 0$.

The calculated levels of the streamline with maximum η $(= \eta_m)$ are below those observed, which probably is another consequence of the differences in the density profiles. This is shown in figure 10 for a particular case. Also shown is the calculated amplitude $\hat{u}$ of the wave-induced horizontal velocity near the free surface and the

† This also explains the smaller wave heights observed near resonance on the ebb during an earlier survey. The gravitational circulation causes relatively low near-bed velocities during ebb tides.

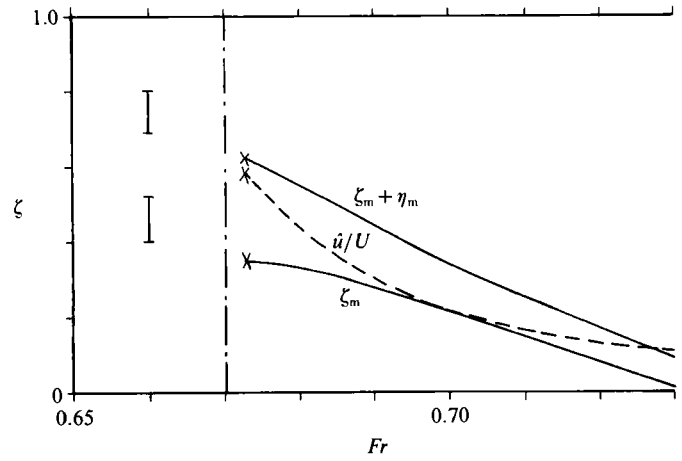

FIGURE 10. Calculated levels of trough and crest of streamline with $\eta = \eta_m$ and wave-induced amplitude of the horizontal velocity versus Froude number for $h = 16.60$ m, $\Delta_b = 0.0831$, $L = 30$ m and $A = 0.07$. The error bars indicate ζ_m and $\zeta_m + \eta_m$ obtained from figure 7 (the error bars of the measured Froude number are not shown). –·–·–, Resonance; ×, onset of gravitational instability.

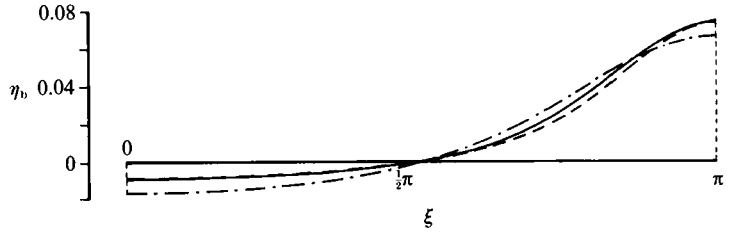

FIGURE 11. Calculated bed profiles (only half the wavelength is shown) for $h = 16.60$ m, $\Delta_b = 0.0831$, $L = 30$ m. ——, $Fr = 0.676$ ($a = 0.02$), $A = 0.07$; – – – –, $Fr = 0.676$ ($a = 0.02$), $A = 0$; –·–·–, $Fr = 0.682$ ($a = 0.04$), $A = 0.07$. Similar profiles obtain for other wavelengths.

bed. Large near-bed velocities may bring on the occasional resuspension of fine sediments (Dyer 1982).

Some calculated bed profiles are shown in figure 11 for $L = 30$ m and Froude numbers close to the Froude number for which gravitational instability occurs. Comparing these profiles with those on the acoustic images shows a fair agreement. Adopting (3.5), the right-hand side of which is the first term of a series expansion obtained by solving (3.1) using the method of separation of variables, therefore is admissible here.

4. Concluding remarks

The increased shear due to internal waves locally reduces the stability of the flow. Calculating the gradient Richardson number from the trapped-wave model of §3.1 yields minimal values (at the location where gravitational instability first arises) of one half in the special case where $A' = 0$ (A arbitrary), and zero in all other cases. It may therefore be expected that the internal waves observed have enhanced the turbulent exchange of mass and momentum, the Reynolds numbers being large. Geyer & Smith (1987) determined gradient Richardson numbers based on mean as

well as instantaneous shear from field observations, and also concluded that including the shear induced by internal waves results in substantially lower values in the halocline. These lower values were consistent with instabilities recorded on their acoustic images. The interfacial mixing appeared to be stronger in a situation with waves, which was attributed to the increased shear production of turbulent kinetic energy.

To increase the limited knowledge of resonant trapped waves in a tidal flow over undular topography, a laboratory experiment would be useful. The inherent time dependence could be obtained by towing a section of undular bottom topography at a gradually decreasing speed (initially supercritical). Alternatively, a slightly supercritical flow could be set up in a flume and the topographical features be allowed to slowly accelerate in the downstream direction. The latter approach would be appropriate if the effect on the turbulence is to be studied.

The field survey was carried out by Rijkswaterstaat, Ministry of Transport and Public Works, from which also financial support was obtained. The writers wish to thank A. van der Wekken and B. Kranenborg of Rijkswaterstaat for their co-operation. One of us (J. D. P.) gratefully acknowledges support from a Royal Society fellowship.

REFERENCES

BAINES, P. G. 1977 Upstream influence and Long's model in stratified flows. *J. Fluid Mech.* **82**, 147.

BAINES, P. G. 1984 A unified description of two-layer flow over topography. *J. Fluid Mech.* **146**, 127.

BELL, T. H. 1975 Lee waves in stratified flows with simple harmonic time dependence. *J. Fluid Mech.* **67**, 705.

CHATWIN, P. C. 1976 Some remarks on the maintenance of the salinity distribution in estuaries. *Estuar. Coast. Mar. Sci.* **4**, 555.

DYER, K. R. 1982 The initiation of sedimentary furrows by standing internal waves. *Sedimentology* **29**, 885.

GEYER, W. R. & SMITH, J. D. 1987 Shear instability in a highly stratified estuary. *J. Phys. Oceanogr.* **17**, 1668.

GRIMSHAW, R. H. J. & SMYTH, N. 1986 Resonant flow of a stratified fluid over topography. *J. Fluid Mech.* **169**, 429.

HUPPERT, H. E. 1980 Topographic effects in stratified fluids. In *Fjord Oceanography* (ed. H. J. Freeland, D. M. Farmer & C. D. Levings) Plenum.

KOOP, C. G. & MCGEE, B. 1986 Measurements of internal gravity waves in a continuously stratified shear flow. *J. Fluid Mech.* **172**, 453.

LANSING, F. S. & MAXWORTHY, T. 1984 On the generation and evolution of internal gravity waves. *J. Fluid Mech.* **145**, 127.

LONG, R. R. 1953 Some aspects of the flow of stratified fluids. I. A theoretical investigation. *Tellus* **5**, 42.

MAXWORTHY, T. 1979 A note on the internal solitary waves produced by tidal flow over a three-dimensional ridge. *J. Geophys. Res.* (C) **84**, 338.

MCDOWELL, D. M. & O'CONNOR, B. A. 1977 *Hydraulic Behaviour of Estuaries.* Macmillan.

MELVILLE, W. K. & HELFRICH, K. R. 1987 Transcritical two-layer flow over topography. *J. Fluid Mech.* **178**, 31.

PIETRZAK, J. D., ABRAHAM, G. & KRANENBURG, C. 1989 Field observations of internal waves in the Rotterdam Waterway. *Stratified Flows Rep.* 6. Rijkswaterstaat, Delft Hydraulics, Delft University of Technology.

PIETRZAK, J. D., KRANENBURG, C. & ABRAHAM, G. 1990 Resonant internal waves in fluid flow. *Nature* **344**, 844.

TURNER, J. S. 1973 *Buoyancy Effects in Fluids*. Cambridge University Press.

YIH, C.-S. 1980 *Stratified Flows*. Academic.